Supplementary Material For

Experimental Verification of Acoustic Pseudospin Multipoles in a Symmetry-Broken Snowflake-like Topological Insulator

Zhiwang Zhang[1], Ye Tian[1], Ying Cheng[1,*], Xiaojun Liu[1,†], and Johan Christensen[2,‡]

Department of Physics, Collaborative Innovation Center of Advanced Microstructures, Nanjing University, Nanjing 210093, China

[2]*Instituto Gregorio Millan Barbany, Universidad Carlos III de Madrid, ES-28916 Leganés, Madrid, Spain*

Email: * chengying@nju.edu.cn; †liuxiaojun@nju.edu.cn; ‡johan.christensen@uc3m.es

Note 1. Pseudo time reversal symmetry

We demonstrate that the time reversal (TR) symmetry is inherent in the present metamaterial lattice with C_6 point group symmetry, which has two 2D irreducible representations: E_1 with basis function (x, y) and E_2 with basis function $(x^2\text{-}y^2, 2xy)$[1]. Importantly, the symmetries of E_1 and E_2 are the same as (p_x, p_y) and $(d_{x^2-y^2}, d_{xy})$ orbits of electrons in quantum systems. The irreducible representations of the rotation operators on basis $(x, y)^T$ are denoted by :

$$D_{E_1}(C_6)=\begin{pmatrix} 1/2 & -\sqrt{3}/2 \\ \sqrt{3}/2 & 1/2 \end{pmatrix} \tag{S1}$$

$$D_{E_1}(C_6^2)=\begin{pmatrix} -1/2 & -\sqrt{3}/2 \\ \sqrt{3}/2 & -1/2 \end{pmatrix}. \tag{S2}$$

We compose the pseudo TR operator

$$\mathrm{T} = \mathrm{UK} = -i\sigma_y \mathrm{K}, \tag{S3}$$

with a unitary operator

$$\mathrm{U} \equiv \left[D_{E_1}(C_6) + D_{E_1}(C_6^2) \right] / \sqrt{3} = \begin{pmatrix} 0 & -1 \\ 1 & 0 \end{pmatrix} = -i\sigma_y, \tag{S4}$$

where σ_y is the Pauli matrix and K is complex conjugate operator.

It follows that

$$\mathrm{T}^2 \begin{pmatrix} p_x \\ p_y \end{pmatrix} = \mathrm{TU} \begin{pmatrix} p_x \\ p_y \end{pmatrix} = \mathrm{T} \begin{pmatrix} -p_y \\ p_x \end{pmatrix} = - \begin{pmatrix} p_x \\ p_y \end{pmatrix}, \tag{S5}$$

which yields $\mathrm{T}^2 = -1$.

Similarly, the irreducible representations of the rotation operators on basis $(x^2\text{-}y^2, 2xy)^T$ are denoted by :

$$D_{E_2}(C_6) = \begin{pmatrix} -1/2 & -\sqrt{3}/2 \\ \sqrt{3}/2 & -1/2 \end{pmatrix} \tag{S6}$$

$$D_{E_2}(C_6^2) = \begin{pmatrix} -1/2 & \sqrt{3}/2 \\ -\sqrt{3}/2 & -1/2 \end{pmatrix}. \tag{S7}$$

The unitary operator can be constructed as

$$\mathrm{U} \equiv \left[D_{E_2}(C_6) - D_{E_2}(C_6^2) \right] / \sqrt{3} = \begin{pmatrix} 0 & -1 \\ 1 & 0 \end{pmatrix} = -i\sigma_y. \tag{S8}$$

We also compose the pseudo TR operator $\mathrm{T} = \mathrm{UK} = -i\sigma_y \mathrm{K}$, which yields $\mathrm{T}^2 = -1$. From the above, the pseudo TR symmetry in the present metamaterial lattice is similar to the TR symmetry of electrons, which guarantees appearance of Krammers doublet at Γ point for present metamaterial lattice with C_6 point group symmetry.

On this basis, we can easily compose the pseudo TR operator $\mathrm{T}' = \mathrm{U}'\mathrm{K}$ on the basis $(p_+, p_-)^T$ with

$$\begin{pmatrix} p_+ \\ p_- \end{pmatrix} = \begin{pmatrix} 1/\sqrt{2} & i/\sqrt{2} \\ 1/\sqrt{2} & -i/\sqrt{2} \end{pmatrix} \begin{pmatrix} p_x \\ p_y \end{pmatrix} = \mathrm{V} \begin{pmatrix} p_x \\ p_y \end{pmatrix}, \tag{S9}$$

in which the transformation matrix

$$\mathrm{V} = \begin{pmatrix} 1/\sqrt{2} & i/\sqrt{2} \\ 1/\sqrt{2} & -i/\sqrt{2} \end{pmatrix}, \quad \mathrm{V}^\dagger = \begin{pmatrix} 1/\sqrt{2} & 1/\sqrt{2} \\ -i/\sqrt{2} & i/\sqrt{2} \end{pmatrix}. \tag{S10}$$

With the unitary operator

$$\mathrm{U}' = \mathrm{V}\mathrm{U}\mathrm{V}^\dagger = \begin{pmatrix} i & 0 \\ 0 & -i \end{pmatrix}, \tag{S11}$$

the pseudo TR operator $\mathrm{T}' = \mathrm{U}'\mathrm{K}$ satisfies

$$\mathrm{T}'^2 p_\pm = \mathrm{T}'\left(\mathrm{m}ip_\mathrm{m}\right) = -p_\pm, \tag{S12}$$

Which gives $\mathrm{T}'^2 = -1$ in irreducible representation E_1. The same conclusion can be discussed on the basis $(d_+, d_-)^T$ with $d_\pm = \left(d_{x^2-y^2} \pm i d_{xy}\right)/\sqrt{2}$ in irreducible representation E_2.

Note 2. Rotating the three-legged rods to induce band inversion

Topological modes inversion takes place when the band gap with two-fold degeneracy closes due to the four-fold degeneracy of double Dirac cones, and then reopens. We demonstrate that the closing-reopening process can be obtained by simply rotating TLRs. The angle shown in Fig. S1(a) is $\phi = 0^o$. Figure S1(b) illustrates that double Dirac cone appears at angle $\phi = -19^o$ and $\phi = 19^o$, of which corresponding dispersion relations are shown in Figs. S1(c)- S1(d). The cone-like dispersion relations will disappear if the range of rotation angle is beyond -30^o~30^o. When rotation angle obeys $-19^o<\phi<19^o$, the "metamolecules" lattice exhibits topologically trivial states and the band gap changes with the different rotation angle. Contrary to this, when rotation angles fulfill $-30^o<\phi<-19^o$ or $19^o<\phi<30^o$, the "metamolecules" lattice exhibit topologically nontrivial states as shown in Fig. S1(b).

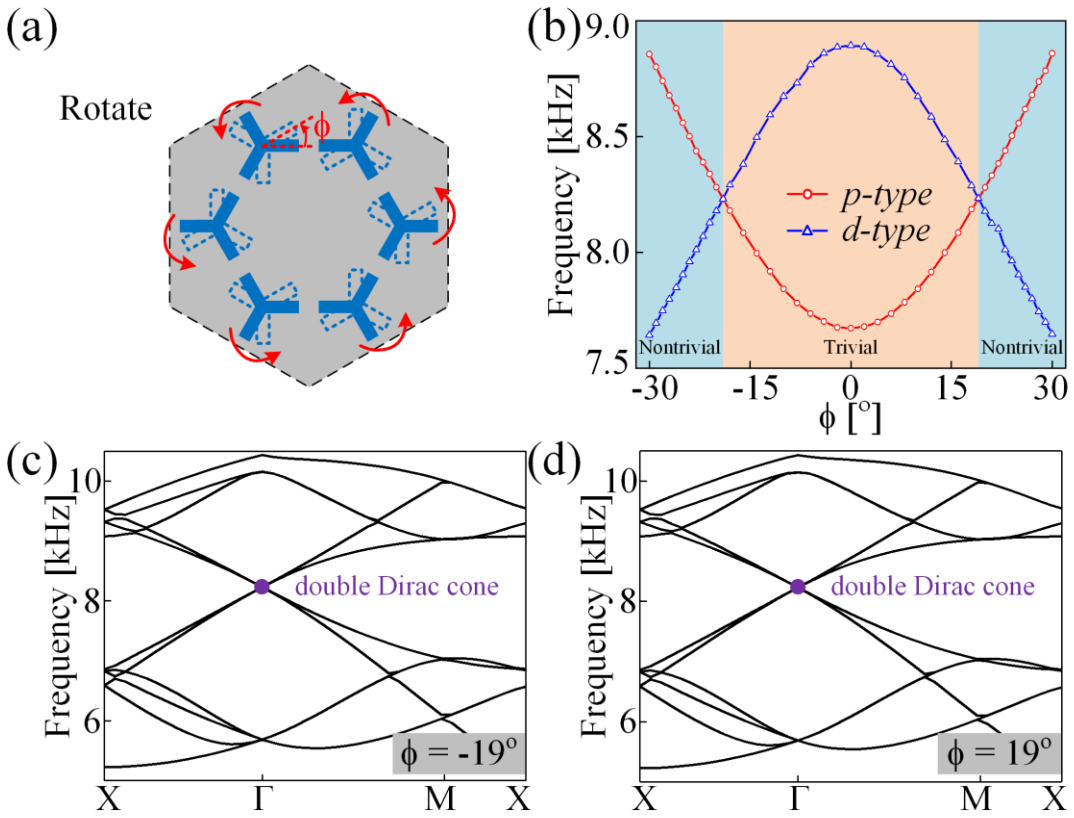

Figure S1 | Rotating the three-legged rods with band inversion. (**a**) Schematic of the metamolecule with the rotation angle ϕ, which is positive/negative when rotating the TLRs anticlockwise/clockwise. (**b**) Eigenfrequencies of the two two-fold degeneracy states near the band gap in dependence to the rotation angle ϕ at the BZ center. The band inversion effect is clearly observed. Corresponding dispersion relations with (**c**) $\phi = -19^{o}$ and (**d**) $\phi = 19^{o}$.

Note 3. Simulations

Numerical simulations were implemented using COMSOL Multiphysics, a finite-element analyzer and solver software. The simulations were performed in the Pressure Acoustic module including the detailed microstructures with the actual geometrical dimensions. The

standard hard wall boundary conditions were applied to the rods. The matrix material applied is air with standard parameters of a mass density $\rho_{\text{air}} = 1.21\ kg/m^3$ and speed of sound $c_{\text{air}} = 343\ m/s$. The largest mesh element size was lower than 1/10th of the shortest incident wavelength. Perfectly matched layers (PML) conditions were imposed on the exterior of the air domain to eliminate interference from the reflected waves.

Note 4. Experiments

The three-legged rods of the PnC were precision-fabricated using epoxy resin via 3D printing. The fabricated PnC sample in Fig. 4a consists of 620 three-legged rods embedded in an air matrix. The height of the rods, which were placed between two parallel plates of Plexiglass, was chosen to be 1.40 cm. In this scenario, the two-dimensional approximation is applicable since the planar waveguide supports propagating mode uniformly along the rod-axis for the wavelengths under consideration. Experiments were conducted by a loudspeaker (ENPILL PD-2121) with a gradual pipe to generate a point sound source. Cone-shaped sound absorbing foam was mounted around the surrounding of the PnC to minimize the boundary reflections by the open space. Local pressure fields were measured by inserting 1/4-inch condensed microphones (GRAS type 40PH) into the top plate at the designated positions. The outputs of the microphones were acquired by a digitizer (NI PXI-4498), and processed by LabVIEW software. A frequency scan was performed from 6.5 kHz to 10.0 kHz with an increment of 0.01 kHz. Highly reliable readings of pressure amplitude at each frequency were ensured by

multiple measurements, from which we obtained the complex transmission/sound intensity by means of the transfer matrix method.

Note 5. Comparison between topological edge states and transmission states

In order to further verify the topological edge states, the sound source at f = 7000 Hz within the transmission states is placed at the interface between the topologically nontrivial and trivial regions for comparison. Fig. S2(a) shows that the source at f = 8200 Hz only allows propagation along the interface with exponential decay into bulk. While the source, at f = 7000 Hz within the transmission states, is placed at the same position, the sounds propagate into the acoustic crystal irregularly, as shown in Fig. S2(b). Therefore, the edge state is protected by the topological properties and it is unidirectional.

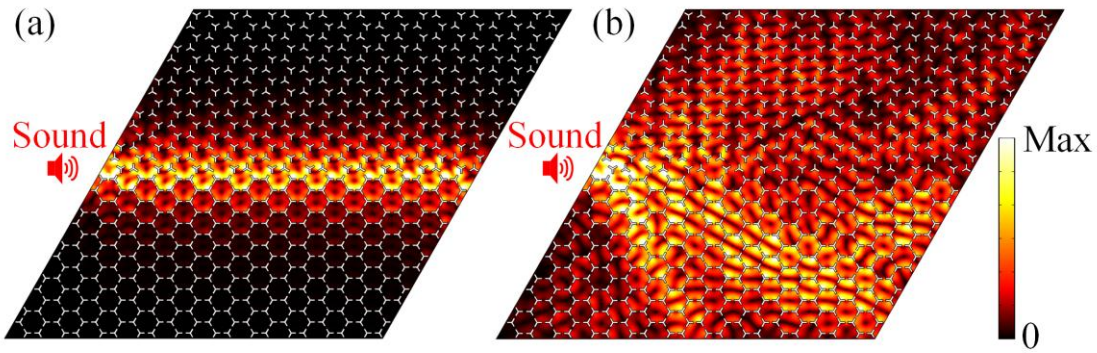

FIG. S2. Comparison between topological edge states and transmission states. The corresponding distributions of acoustic absolute pressure fields excited by the source at **(a)** f = 8200 Hz for topological states, and **(b)** f = 7000 Hz for transmission states.

References

1. L.-H. Wu and X. Hu, Physical Review Letters **114** (22), 223901 (2015).